

## Satellite-derived vegetation index and cover type maps for estimating carbon dioxide flux for arctic tundra regions

Douglas Stow<sup>a,\*</sup>, Allen Hope<sup>a</sup>, William Boynton<sup>a</sup>, Stuart Phinn<sup>a</sup>, Donald Walker<sup>b</sup>, Nancy Auerbach<sup>b</sup>

<sup>a</sup> *Department of Geography, San Diego State University, San Diego, CA 92182-4493, USA*

<sup>b</sup> *Institute of Arctic and Alpine Research, University of Colorado, Boulder, CO 80309, USA*

Received 15 June 1996; revised 31 March 1997; accepted 29 May 1997

### Abstract

The spatial variability and co-variability of two different types of remote sensing derivatives that portray vegetation and geomorphic patterns are analyzed in the context of estimating regional-scale CO<sub>2</sub> flux from land surfaces in the arctic tundra. For a study area encompassing the Kuparuk River watershed of the North Slope of Alaska, we compare satellite-derived maps of the normalized difference vegetation index (NDVI) generated at two different spatial resolutions to a map of vegetation types derived by image classification of data from the Landsat multispectral scanner (MSS). Mean values of NDVI for each cover type stratum are unique (with the exception of moist acidic tundra and shrubland types). Based on analysis of semi-variograms generated for SPOT-NDVI data, most of the vegetation cover and landform features of this arctic tundra landscape have spatial dimensions of less than 1 km. Thaw lakes on the coastal plain and glacial depositional landforms, such as moraines in the foothills, seem to be the largest features, with vegetation units having dimensions no larger than 700 m. Frequency distributions of NDVI and vegetation types extracted for sampling transects flown by an aircraft sensing CO<sub>2</sub> flux, relative to distributions for the entire Kuparuk River watershed, suggest a slight sampling bias towards greater cover of mesic wet sedge tundra and thaw lakes and associated lower NDVI values. The regional pattern of NDVI for the North Slope of Alaska corresponds primarily to differences between the two major physiographic provinces of this region. © 1998 Elsevier Science B.V.

*Keywords:* arctic tundra; remote sensing; carbon dioxide; regional scaling; satellite imagery; spectral vegetation indices

### 1. Introduction

Knowledge of the recently measured increase in the concentration of global carbon dioxide (CO<sub>2</sub>) in the atmosphere combined with the uncertain possible

responses of Earth systems to increases in the atmospheric concentration of CO<sub>2</sub> and other “greenhouse gases” have accelerated research that improves understanding and prediction of the carbon balance for a range of spatial scales (Oechel et al., 1993). In particular, regional-scale to whole biome estimates of net CO<sub>2</sub> and methane (CH<sub>4</sub>) flux from land surfaces are needed for global carbon budgets and as input to global circulation models (Vourlitis and

\* Corresponding author. E-mail: stow@mail.sdsu.edu

Oechel, 1997; Weller et al., 1995). For regional-scale estimates of carbon flux, vegetation distributions and landform patterns are likely to be important indicators of carbon fluxes, because they both control and relate to the dominant mechanistic elements of carbon uptake and release, which are photosynthesis and respiration rates, soil carbon storage, and soil moisture (Oechel and Vourlitis, 1996).

Remote sensing from airborne and/or satellite platforms can provide spatially-continuous data on vegetation and geomorphic patterns which may be utilized to predict regional- to biome-scale patterns of carbon flux. As for most remote sensing applications, three requirements must be met for carbon flux or storage patterns to be predicted based on remote sensing data. First, unique reflective or emissive electromagnetic signatures need to exist and correspond to variations in vegetation and geomorphic patterns. Another requirement is that one or more models are needed to transform values of remotely sensed data into some derivative variable pertaining to the type or condition of land cover and then to estimate carbon flux from this derivative variable. The third requirement is that measurements of carbon flux rates or storage amounts, which are inherently sparse in space, are available to calibrate and validate the models which are used to estimate the distribution of carbon flux from remotely sensed data. Thus, remotely sensed data covering regional extents combined with models provide a means for interpolating between or extrapolating beyond (in a spatial sense) more direct measurements of carbon balance variables. The bases for this interpolation or extrapolation are that: (1) vegetation and geomorphic patterns are indicators of carbon balance regimes, and (2) spatially-continuous remote sensing data can be transformed into reliable maps of vegetation and geomorphic distributions. (Note that remote sensing derivatives are “maps”, if the image data from which they were derived have been referenced to Earth coordinates by way of geometric image processing.)

The focus of this paper is on the analysis of spatial variability and co-variability of two different types of remote sensing derivatives which portray vegetation and geomorphic patterns, in the context of estimating regional-scale CO<sub>2</sub> flux from land surfaces of the arctic tundra biome. One type of deriva-

tive is a map of the normalized difference vegetation index (NDVI), where NDVI is the difference between near infrared and red waveband radiance or reflectance divided by the sum of radiance or reflectance for these two wavebands. NDVI maps are derived from near infrared and red (or broad visible) waveband images acquired by optical, multispectral sensors. Another type of derivative is a map of classified vegetation and other land cover types (which will be referred to as vegetation type throughout this paper for succinctness). Maps of vegetation types are most commonly derived by subjecting optical, multispectral image data to statistical algorithms for pattern recognition. Whereas both derivative products are spatially-continuous maps portraying vegetation and geomorphic patterns, NDVI is a continuous (numerical and ratio-scale) variable and vegetation type is a discrete (categorical and nominal-scale) variable. Here, we examine the spatial variability of NDVI at two different spatial scales and the manner in which NDVI maps correspond to a map of vegetation types for a study area on the North Slope of Alaska. These data sets provide a means for determining if transects flown by an aircraft with CO<sub>2</sub> flux measuring sensors are representative of vegetation distributions and possibly, the flux regimes, for an entire watershed which encompasses these transects. Also, the data sets enable analyses into the appropriate spatial scales of sampling CO<sub>2</sub> flux and NDVI based on landscape-scale vegetation and landform variability. Finally, we examine the influence of geomorphic features on the spatial pattern of NDVI, at fine, landscape and regional scales.

## 2. Background

These research results stem from our more comprehensive study of whether NDVI data can be integrated with scaling models to yield realistic regional estimates of net CO<sub>2</sub> exchange from arctic tundra surfaces over large regions. The scaling models extend measurements of CO<sub>2</sub> flux made at three different spatial scales using closed-top chambers (Oechel et al., 1993), micrometeorological eddy flux towers, and very-low flying aircraft with eddy flux instrumentation operated by the National Oceanic

and Atmospheric Administration (NOAA) Atmospheric Turbulence and Diffusion Division (ATDD), Oak Ridge, Tennessee, to estimate regional flux (Hope et al., 1995). These measurements of CO<sub>2</sub> flux and our studies of NDVI for regional estimates of CO<sub>2</sub> flux are being conducted as part of a large collaborative project sponsored by the National Science Foundation called the Land–Atmosphere–Ice–Integration (LAI) FLUX study. The purpose of LAI-FLUX is to improve scientific understanding of controls and rates of carbon, energy, and water flux from and between terrestrial, aquatic, and atmospheric systems in the Arctic (Weller et al., 1995). Other LAI-FLUX researchers are developing models for extending in space (watersheds to biome) and time (days to entire growing season) the measurements of CO<sub>2</sub> flux made at the three spatial scales and several temporal frequencies (Oechel et al., 1996). NDVI and/or vegetation type data are being incorporated into some of these models as a means for extrapolating in space and time, more direct measurements of CO<sub>2</sub> flux.

Spatial variations of spectral vegetation indices, such as the NDVI, relate to variations in plant composition and abundance for shrubs and sedges in arctic tundra environments. Hope et al. (1993) analyzed ground-level spectral radiometric data in relation to detailed plant composition and biomass data and found that photosynthetic biomass and green plant cover of moist tussock tundra explain most of the variance in NDVI. Near infrared reflectance and, therefore, NDVI, seems to be most sensitive to the amount of green foliar cover of dwarf shrubs (Hope et al., 1993). Supporting this statement and also based on ground-level spectral radiometry, the study by Vierling et al. (1997) showed that NDVI based on off-nadir measurements of spectral reflectance are more sensitive to the amount of woody, dwarf shrub cover than NDVI from nadir measurements. Results from Stow et al. (1993a) and Shippert et al. (1995) demonstrated that, for the foothills province of the North Slope, mean NDVI values derived from field radiometry and SPOT multispectral (XS) image data for corresponding areas of arctic tundra vegetation types co-varied in a linear manner. Stow et al. (1993a,b) also found that NDVI values derived from SPOT XS data were generally unique for each of the major vegetation types occurring in the North Slope

foothills. Walker et al. (1995a) supports this finding and also demonstrates a significant difference in NDVI values for acidic and non-acidic types of moist tundra vegetation which have developed on glacial terrain of different ages and soil characteristics.

Spectral vegetation indices have been used to estimate carbon fluxes at a variety of spatial scales. Global-scale estimates of atmospheric draw-down of CO<sub>2</sub> and aboveground gross primary production have been made using the NDVI (Tucker et al., 1986; Tucker and Sellers, 1986; Fung et al., 1987). Plot level estimates of CO<sub>2</sub> exchange, based on the same index, have been made in the sub-arctic by Whiting et al. (1992). For many ecosystems, respiration tends to be a small and relatively constant fraction of net ecosystem carbon exchange (NEE), so relationships between the NDVI and NEE mainly reflect the relationship between carbon assimilation or gross primary production (GPP) and the spectral index. In the Arctic tundra regions of Alaska, ecosystem respiration (ER) is, however, a significant and variable component of NEE. McMichael (1995) examined the relationship between NDVI and NEE, GPP and ER using data collected over small plots (0.75 m<sup>2</sup>) and found no relationship between NDVI and NEE but significant relationships between NDVI and GPP and ER. Furthermore, these relationships were different for the coastal plain and foothills provinces of the North Slope.

The classification and mapping of arctic tundra vegetation is a subject which is important to studies pertaining to biogeochemical cycling and landscape ecology such as this one and also, to wildlife habitat, ecosystems, hydrology, and general resource management applications in the arctic. Much effort has gone into the development of standardized systems of vegetation classification (Walker et al., 1995b) and classification techniques which exploit moderate resolution satellite data from Landsat multispectral scanner (MSS) (Walker and Acevedo, 1987; Shasby and Carnegie, 1986) and SPOT multispectral (XS) (Stow et al., 1989) systems. Satellite-based approaches to classification and mapping are necessary given the large expanses of arctic tundra lands which are difficult to access and rarely are covered by suitable aerial photography (Walker et al., 1995b).

The study area for this investigation is defined by

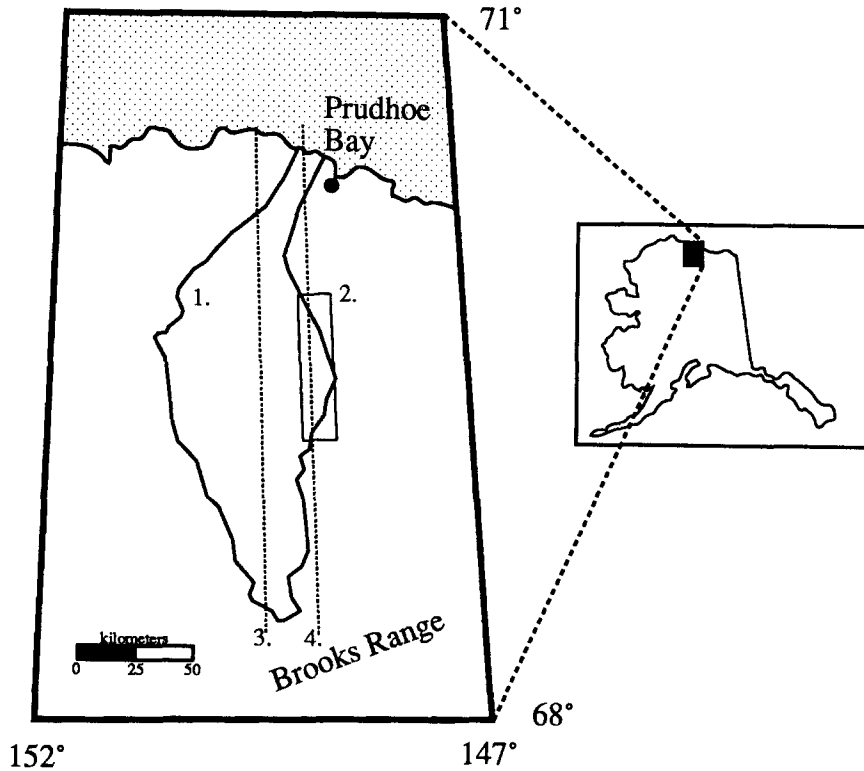


Fig. 1. Study area map for a portion of the North Slope of Alaska. Outlined on the map are several subareas from which NDVI and/or vegetation type data were extracted for analysis: (1) the Kuparuk River watershed; (2) N–S trending rectangle used as the SPOT NDVI “transect” sampling set for semi-variogram analysis; (3) and (4) two N–S transects established for NOAA-ATDD flux aircraft sampling.

a rectangle which contains the boundary of the Kuparuk River watershed located within the region known as the North Slope of Alaska (Fig. 1). A portion of the Sagavanirktok River and its watershed is also covered by the rectangular study area. Characteristic of the North Slope, the topography of the Kuparuk River watershed trends from the steep descent from the Brooks Range mountains at the extreme south, across rolling foothills composed of glacial moraine deposits and flattens out onto an expansive coastal plain which slopes gently to the Arctic Sea. Periglacial landform features dominate the physical landscape. Thaw lakes and patterned ground are the most characteristic features of the coastal plain. The harsh arctic climate of the study area is characterized by a long (8- to 9-month) period of snow cover with a short snow-free period from end of May to the beginning of September. The vegetative growing season and partial thawing of the

permafrost occurs during this 3- to 4-month snow-free period. Communities of arctic tundra vegetation vary across a moisture gradient from wet sedge to moist tussock to dry lichen tundra. Shrub tundra and riparian vegetation occurs in water track drainages and along small stream channels and river flood plains. Unlike most of the North Slope region, human activities are evident throughout the study area in the form of the Trans-Alaskan pipeline and associated haul road (Dalton Highway), sand and gravel excavation sites adjacent to the haul road, and the relatively intensive oil exploration and processing facilities of the Prudhoe Bay oil fields.

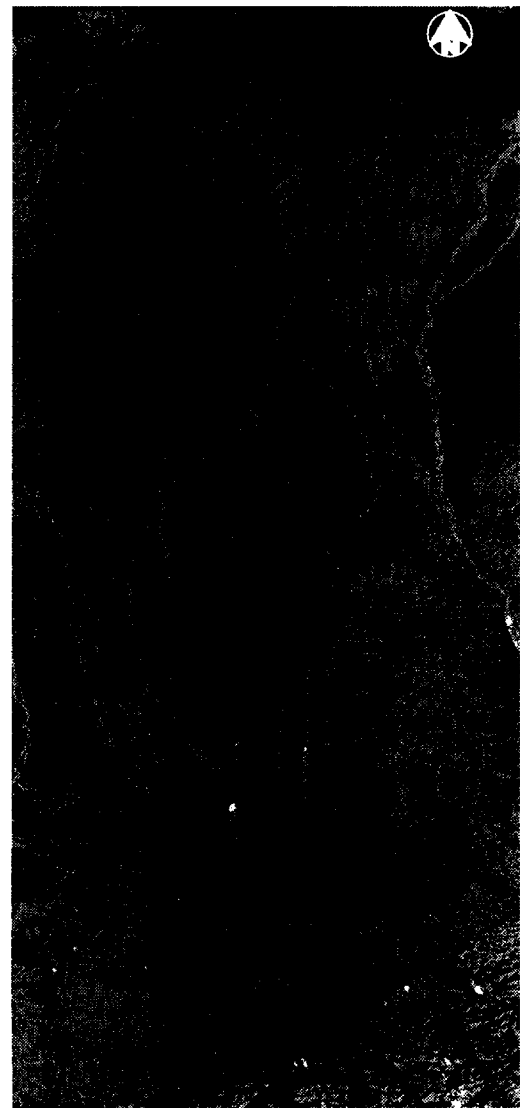
### 3. Data and methods

We compared satellite NDVI maps for the Kuparuk River watershed generated at two different

spatial resolutions to a general map of vegetation types derived by image classification of Landsat multispectral scanner (MSS) data. Descriptive, inferential, and spatial statistics were generated to assess spatial variability and co-variability of NDVI and vegetation types at landscape scales throughout the Kuparuk River watershed.

### 3.1. Landsat MSS data and processing

General vegetation landcover types were derived by image classification of Landsat MSS data. Derived classes include (1) barrens, (2) moist non-acidic tundra and dry tundra, (3) moist acidic tundra, (4) shrublands, (5) wet tundra, (6) water, (7) clouds and ice, and (8) shadows. To expedite image processing, the digital data for a rectangular region encompassing the Kuparuk River watershed were extracted from an existing mosaic of MSS frames covering the Central Arctic Management Area (CAMA) and Arctic National Wildlife Refuge (ANWR), Northeast Alaska, produced by the National Mapping Division, U.S. Geological Survey, EROS Data Center, Sioux Falls, SD. Images for the entire mosaic were acquired through the snow-free growing seasons of 14 August, 1976 through 2 August, 1985. Because of prevalent cloud cover over the North Slope during most growing seasons, single time period (e.g. 1 week) mosaics of imagery from sun-synchronous satellites are generally not feasible. The mosaic (80 m nominal spatial resolution) data set was resampled to 50-m pixels using a cubic convolution interpolation when applying a second-order polynomial warping function for purposes of geographically referencing the image data. An ISODATA iterative clustering routine was run using green, red, and infrared wavebands of the MSS image. As part of the implementation of this unsupervised classification approach, forty cluster classes were initially generated and then aggregated into eight land cover classes. Geobotanical maps and earlier Landsat-derived maps of the region were used for supplementary information to interpret the spectral classes (Walker and Acevedo, 1987; Walker and Walker, 1991, 1996). The MSS classification was further calibrated and refined with field and low-level helicopter observations. The digital map of vegetation types analyzed in this study is shown in Fig. 2.



0 50 Kilometers

#### Vegetation Cover Types

-  moist acidic tundra
-  water & shadows
-  moist non-acidic tundra
-  shrublands
-  wet tundra
-  barrens
-  clouds & ice

Fig. 2. Landsat MSS-derived map of vegetation types (Walker).

### 3.2. NOAA AVHRR data and processing

Coarse-scale NDVI values (ca. 1 km spatial resolution) were derived from NOAA 11 AVHRR data acquired at near-nadir viewing angles within two hours of the SPOT data. The data had been geometrically and radiometrically processed by the Alaska Data Visualization and Analysis Laboratory, University of Alaska Fairbanks Center. A systematic geometric correction which incorporates attitude and position data in the AVHRR ephemeris had been applied, along with a radiometric calibration based on published radiance coefficients. In an attempt to normalize AVHRR brightness values between bands and relative to the SPOT data, we applied a linear transformation based on a number of pixel samples extracted for near-homogeneous features from both images. An NDVI transformation was applied and two subsets were extracted from: (1) a rectangular region oriented north-south and east-west which encompasses the Kuparuk River watershed (Fig. 3A), and (2) a rectangular region with transverse orientation to correspond with the SPOT mosaic.

### 3.3. SPOT XS data and processing

Two adjacent SPOT multispectral (XS) image frames acquired along a single satellite orbit on 31 July, 1994 provided an intermediate-scale source for deriving NDVI maps at a spatial resolution of 20 m. These two SPOT frames, which only covered a portion of the Kuparuk River watershed, were the only moderate resolution satellite image data, i.e. SPOT, Landsat thematic mapper (TM) or Indian Remote Sensing (IRS), available for the study area for the 1994 and 1995 growing seasons. The images were acquired in Level 1B geometric format, meaning that they had been subjected to geometric processing routines to correct for systematic errors associated with sensor operation and earth motion and curvature. We applied image warping functions to rectify and georeference the two SPOT frames based on ground control points derived from 1:63 360-scale topographic maps. Radiometric normalization was also performed by applying calibration factors for spectral radiance (provided by SPOT Image Corp.) and normalizing for between-band atmospheric effects using the improved dark object subtraction

method developed by Chavez (1988). The two georeferenced and radiometrically normalized frames were then joined to create a seamless mosaic. A digital NDVI map was generated from this mosaic and is shown in Fig. 3B.

### 3.4. Statistical and graphical analyses

Sample sets of NDVI values from the two variable-scale maps and vegetation categories from the classified MSS image were drawn based on several spatial-categorical criteria and subjected to statistical routines. The primary spatial features that were utilized as a basis for sampling were: (1) vegetation units defined by rectangular areas that were at least  $3 \times 3$  km and mostly homogeneous in terms of vegetation composition according to the MSS-derived vegetation map, (2) two 6-km wide transects corresponding to the NOAA-ATDD flux aircraft flightlines on the W148°55' and W149°30' longitudinal lines, (3) one 67-km long by 15-km wide transect oriented north, (4) three subdivisions of this transect, divided into coastal plain, transition and foothill zones, and (5) the Kuparuk River watershed. Sampling by vegetation criteria was performed for: (1) large land units composed of a predominant vegetation type, and (2) pixel-by-pixel stratification of SPOT and AVHRR-derived NDVI maps based on vegetation type.

Parametric statistics and frequency distribution plots were generated for many of these sample sets. Analysis of variance (*F*-test) was applied to determine if vegetation types had unique NDVI signatures.

A semi-variance routine (Curran, 1988) was run on the NDVI sample sets that were based on vegetation units and the major N–S transect. Semi-variances were computed on the Cray C90 of the San Diego Supercomputer Center to derive isotropic semi-variograms for relatively large sample sets. The routine was also applied to a detrended version of the transect sample set. The detrending was achieved by stratifying by vegetation type and then subtracting the mean NDVI for each vegetation type from the NDVI image on a pixel-by-pixel basis (Davis et al., 1989). Resultant semi-variograms were analyzed to assess scale-dependent variation of NDVI for these sample sets (Curran, 1988). In addition, comparisons

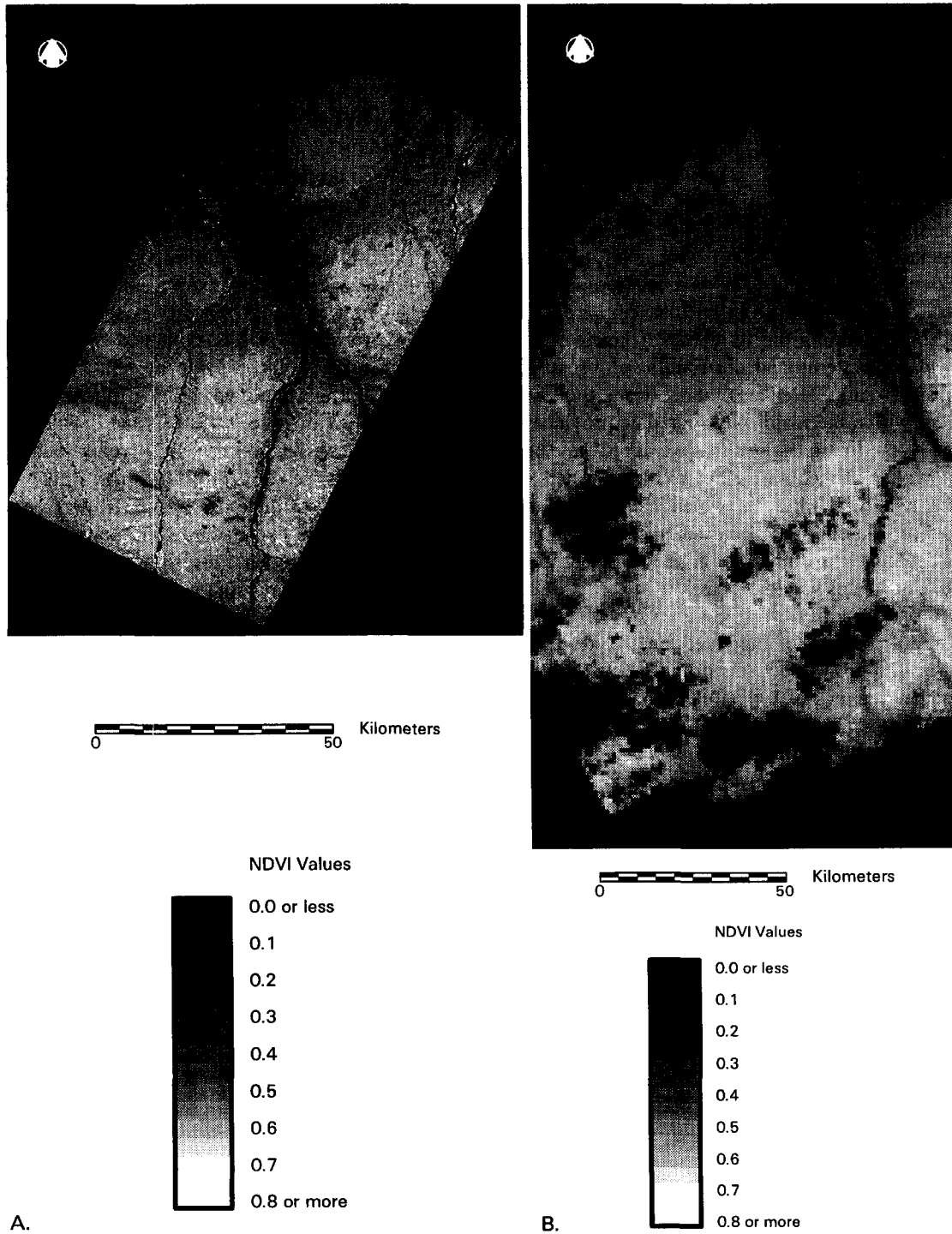


Fig. 3. Satellite-derived NDVI maps for the Kugaruk River watershed. (A) NDVI map from SPOT XS image frames acquired 31 July, 1994, and (B) NDVI map from NOAA AVHRR orbital segment acquired 31 July, 1994.

of the magnitude of the universal variance of original and detrended versions of NDVI sample sets provided insight into the amount of NDVI variance explained by the spatial variability of vegetation types.

#### 4. Results

The spatial patterns and degree of correspondence of vegetation types and NDVI were analyzed in the context of extrapolating CO<sub>2</sub> flux measurements to estimate regional flux. A particular emphasis was placed on examining the influence of landforms on these spatial patterns and determining if vegetation composition and NDVI magnitudes were similar or different within the major physiographic provinces.

One of the first questions that we asked was: how representative of the entire Kuparuk River watershed are the two N–S transects which had been established for making CO<sub>2</sub> measurements from the NOAA-ATDD flux aircraft? While eventually we would like to answer this question in terms of the characteristics of CO<sub>2</sub> flux, comparisons of the frequency distributions of the satellite-derived vegetation type and NDVI data sets provides an indication of whether regimes of CO<sub>2</sub> flux along the transects may be comparable to those of the entire watershed.

The frequency of occurrence of vegetation types is expressed as percent cover of each transect, both

transects combined and the watershed for each of the six cover types in Fig. 4. According to the MSS-derived classification, moist non-acidic tundra is the predominant cover type for the watershed and the transects, closely followed by moist tussock tundra. For the W149°30' transect the two moist tundra types nearly cover equal proportions at around 32%. The cover proportions intersected by the W149°30' transect are more similar to the proportions for the entire watershed than the W148°55' transect. The most substantial difference in cover proportions for the transects relative to the watershed is the higher amount of wet tundra types (wet sedge and shrublands) and water. This is explained by the transects being located within a large portion of the poorly drained, thaw lake covered fluvial plains and deltas associated with the Kuparuk and Sagavanirktok Rivers. These features occupy proportionally less area in the entire Kuparuk River watershed.

Frequency distributions of AVHRR-derived NDVI extracted for the two transects and the entire watershed were analyzed and are shown as histograms in Fig. 5. The most obvious feature of the three histograms is the bimodal distribution of NDVI; one mode is centered at 0.25 and the other near 0.40. By displaying the locations of pixels with NDVI values falling within the intervals corresponding to these two modes, we determined that the modes are mostly associated with the two major physiographic provinces, the coastal plain having the higher NDVI

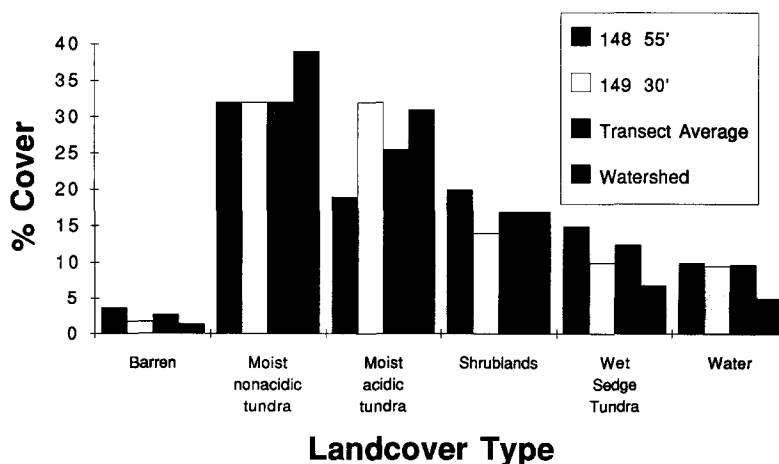


Fig. 4. Percent cover of vegetation and land cover types derived from the Landsat MSS classification for the Kuparuk River watershed relative to proportions along the two NOAA-ATDD flux aircraft transects.

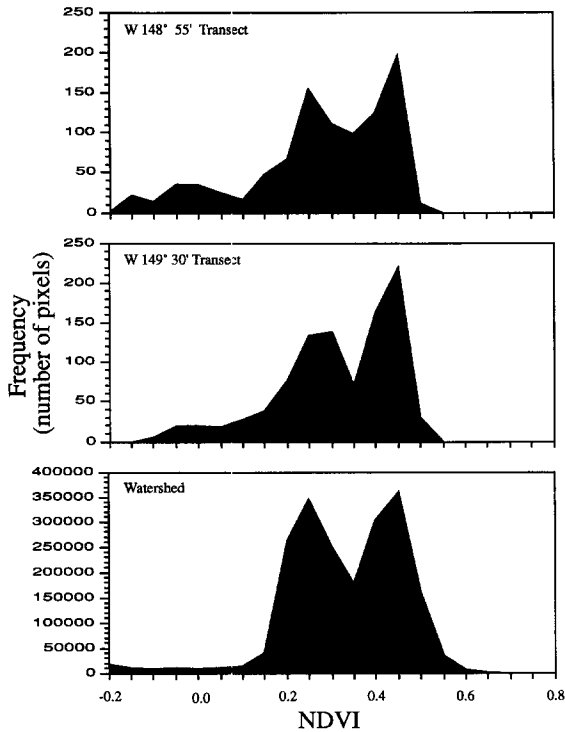


Fig. 5. Frequency distribution of NOAA AVHRR NDVI values extracted for pixels representing the Kuparuk River watershed and the two NOAA-ATDD flux aircraft transects.

values. The major difference between the NDVI frequency distributions of the transects relative to the watershed is the greater frequency of occurrence of pixels associated with low values and the lower frequency of pixels associated with the mode centered at  $NDVI = 0.25$ . As suggested by the findings pertaining to proportional cover discussed above, these distributional differences are likely associated with the greater water and wet sedge types (lower NDVI) intersected by transects relative to the higher proportion of non-acidic tundra (higher NDVI) within the watershed. Also consistent with the differences in the proportions of vegetation types is the fact that the NDVI distribution for the  $W149^{\circ}30'$  transect is more similar to the watershed distribution than the  $W148^{\circ}55'$  transect.

Profiles of AVHRR-derived NDVI for the entire length of both transects and from SPOT-derived NDVI for much of the  $W148^{\circ}55'$  transect provide an

opportunity to assess north–south variation in NDVI across the North Slope (Fig. 6). All three transects exhibit a similar trend; level or slightly increasing from south to north across the foothills province, a steadily decreasing transition zone, a level to slightly decreasing zone corresponding to the coastal plain province, and then an abrupt decline at the Arctic Sea coast. High frequency dips in the NDVI profiles are evident for the coastal plain zone (particularly in the finer spatial resolution SPOT NDVI transect), where the transects intercept thaw lakes and other bodies of water (Morrissey and Livingston, 1992). Other dips correspond to flood plain sediments of rivers cutting across the transects, and patchy clouds.

The spatial correspondence of satellite-derived NDVI distributions relative to that of vegetation type was assessed by stratifying the SPOT NDVI map by the classification map of vegetation types. Fig. 7 portrays the mean ( $X$ ) and standard deviation ( $S_x$ ) of red and near-infrared spectral radiance and NDVI values for each cover type class. NDVI values for vegetation types were normally distributed, while those for barren and water types were bimodal. As is generally the case, NDVI for the vegetation types was mostly influenced by near-infrared radiance. Mean values for vegetation types ranged from 0.37 for wet sedge tundra to 0.57 for moist acidic tundra. The coefficient of variation ( $S_x/X$ ) for the vegetation types varied between 20% and 25%, and was greater than 100% for barren and water. The bimodality and high variance in NDVI for “barren” and “water” types resulted from misregistration and differences in pixel size between the NDVI and cover type maps. Also, most of the “barren” pixels corresponded to the wide Sagavanirktok River plain which is composed of coarse sediment, riparian vegetation and water. For the “water” pixels, higher than normal NDVI values and variance can be explained by relatively high reflectance from marl lakes and possible differences in the extent of water bodies between the dates of Landsat and SPOT image acquisitions.

Results from analysis of variance ( $F$ -tests) showed that, except for one case, mean values of NDVI were significantly different for pairs of cover type classes. As was visually evident from Fig. 7, the moist acidic tundra and shrubland classes had similar NDVI mean values. These types occur in the same portions of the

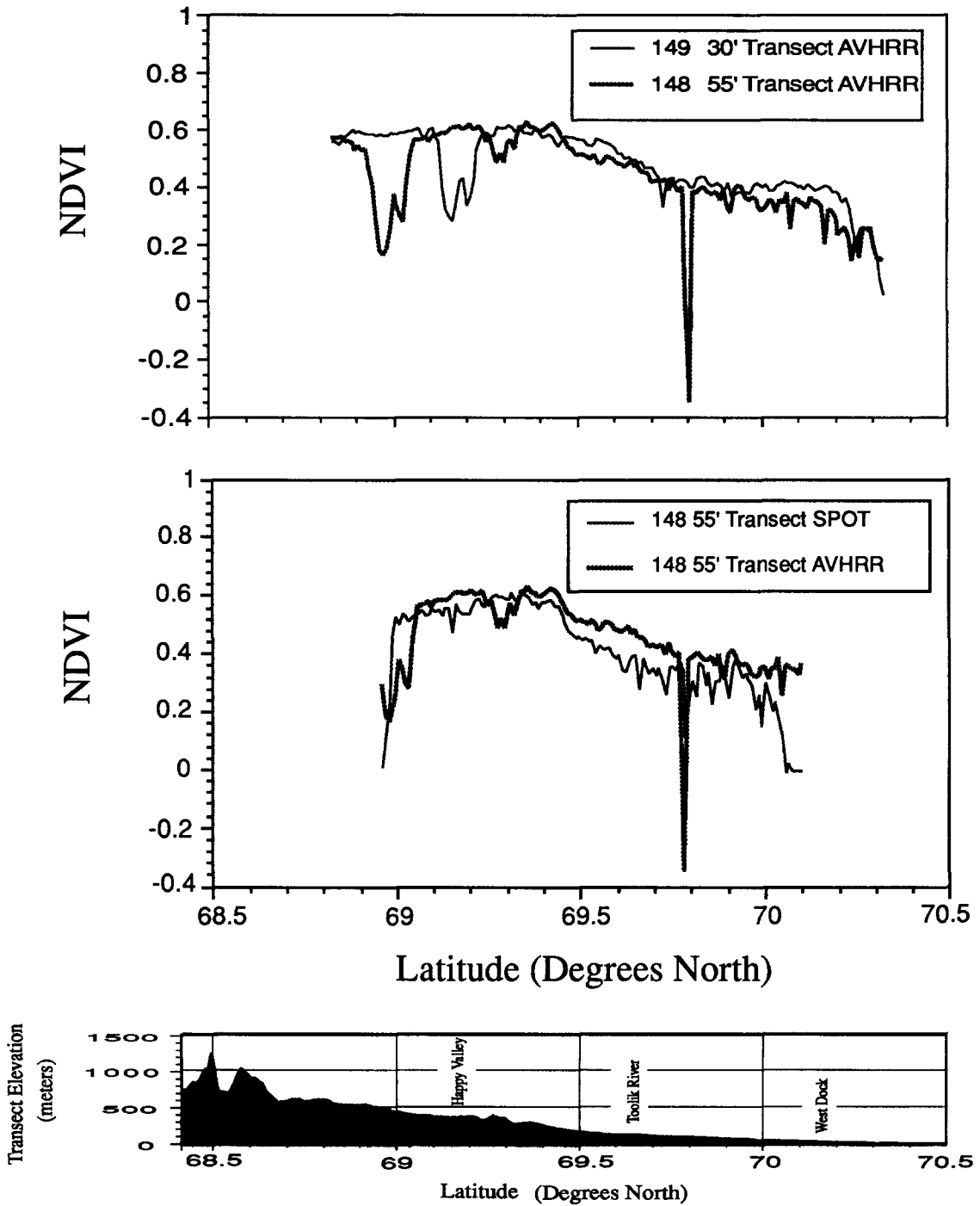


Fig. 6. Spatial variation of NDVI along N–S transects. (a) NDVI from NOAA AVHRR comparing W148°55' and W149°30' transects; (b) NDVI from SPOT XS and NOAA AVHRR for a common segment of the W148°55' transect.

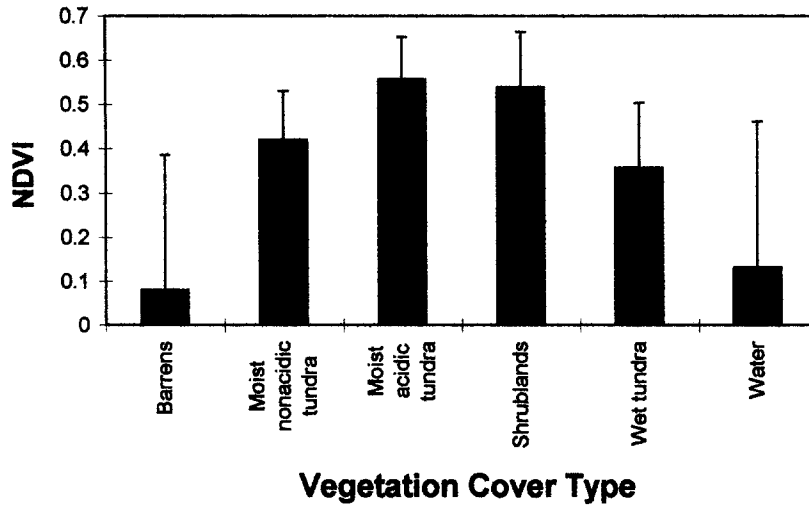


Fig. 7. Mean and standard deviation of SPOT XS-derived NDVI values for vegetation strata.

Kuparuk River watershed and have similar composition of vegetation species, with the main difference being a greater proportion of dwarf shrubs for the shrubland class. Also, misregistration and differences in spatial resolution between the vegetation cover type and NDVI maps have likely resulted in a reduction in NDVI magnitude for the “shrubland” class which tends to occur in small, heterogeneous patches. Though NDVI means were determined to be significantly different for barren and water versus all other classes (as one would expect, given the dissimilar spectral reflectance properties), the *F*-test results should be viewed with caution given the bi-modal NDVI frequency distributions for these classes.

Analysis of semi-variograms computed from SPOT NDVI sample sets provided much insight into the spatial structure of the arctic tundra landscape within the Kuparuk River watershed. The most informative diagnostic features of the semi-variograms were the range and the characteristic form. The range is the lag distance or spatial scale at which the semi-variance stabilizes and asymptotically approaches the regional variance or sill. The characteristic form describes the overall shape of the variogram (e.g. spherical or exponential) as it approaches the sill from smaller lag distances.

Semi-variograms of NDVI sample sets that represented homogeneous vegetation units had very different forms for differing vegetation types. Examples

of characteristic semi-variograms depicting the standardized semi-variance as a function of lag distance (Woodcock et al., 1988) for each of the four general vegetation types are shown in Fig. 8. The standardized semi-variance was computed by dividing the semi-variance by the overall variance for the entire NDVI sample set. For moist acidic and non-acidic tundra and wet sedge tundra, the semi-variograms tend to reach their ranges at a lag distance of 200 to 400 m. For shrub tundra, the range is closer to a distance of 600 to 700 m. Variograms for wet sedge and moist acidic tundra rise steeply and bend sharply as they approach their sills, which signals a high

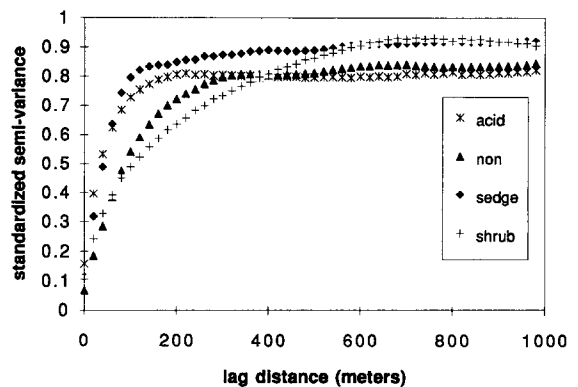


Fig. 8. Standardized semi-variograms of NDVI sample sets extracted from large land units of homogeneous vegetation composition.

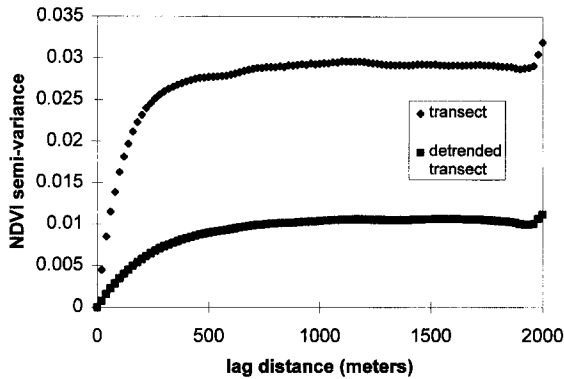


Fig. 9. Semi-variograms of NDVI sample sets (original and detrended by vegetation types) extracted from N–S trending transect.

frequency (60 to 120 m) landscape pattern (Cohen et al., 1990). We attribute this to: (1) higher-order pattern features associated with aggregates of high- and low-centered polygons in the wet sedge tundra of the coastal plain (Belchansky et al., 1995), and (2) linear watertrack drainage features of higher shrub cover that traverse across the tussock tundra dominated acid tundra vegetation type in the foothills province (Stow et al., 1993a). The non-acidic tundra exhibits little landscape variation at high spatial frequencies at the 60 to 120 m scale of the NDVI series. The larger range of the shrub tundra variograms may be explained by the shrub dominant sample sets being composed of subunits with characteristic dimensions of 200 to 400 m. These subunits have homogeneous internal shrub cover proportions but differing shrub proportions between units.

We found the isotropic semi-variograms to be a useful tool for examining spatial structure at the landscape scale and the amount of overall NDVI variance explained by patterns of vegetation types. Fig. 9 shows the semi-variograms for the N–S trending NDVI transect sample set and for the detrended version of this same set. The range of both semi-variograms occurs at about 800 to 1000 m. The semi-variogram of the original transect sample set exhibits a slight leveling then secondary rise in the 500 to 700 m lag distance interval. This is likely indicative of the size of dominant meso-scale landform features within the transect, such as thaw lakes in the coastal plain and the narrow dimension of the

moraines in the foothills provinces. Large hills in the vicinity of Happy Valley have been interpreted by Hamilton (1986) as mid-Pleistocene (Sagavanirktok I) moraines. Most of these moraines are very large features in the order of 500 to 1000 m wide and many kilometers long. In Fig. 9, one can also see from the difference between the variograms of the original and detrended transect sample sets, that roughly two-thirds of the spatial pattern of NDVI is accounted for by the variability of vegetation/land cover types.

## 5. Discussion and conclusion

Because the SPOT-derived NDVI and the vegetation type data are derived from moderate-resolution satellite multispectral data, the two data sets may be providing similar (and possibly, redundant) information pertaining to CO<sub>2</sub> flux regimes. Mean values of NDVI for each cover type are unique (with the exception of moist acidic tundra and shrubland types) and the spatial variability of NDVI within cover type units is often great because of abiotic and biotic heterogeneity. The approximately one-third reduction of semi-variance for the detrended (by vegetation type) NDVI data relative to the original NDVI transect sample set also implies a high degree of correlation or redundancy between the NDVI and vegetation type maps. The variance of NDVI within vegetation type strata is likely caused by the variability of plant cover, biomass, and/or leaf area index, particularly with respect to variations in dwarf shrubs (Shippert et al., 1995). The magnitude of the within-class NDVI variance, however, is likely to be exaggerated, as a result of misregistration between the two satellite-derived maps and classification errors in the map of vegetation types.

Advantages and disadvantages are associated with satellite-derived NDVI and vegetation type maps as bases for estimating regional CO<sub>2</sub> flux. Maps of NDVI are relatively simple to generate from an image processing standpoint, with the primary requirement being radiometric calibration and normalization. In contrast, to generate a realistic map of vegetation types requires numerous processing iterations of statistical pattern recognition, knowledge of

the vegetation and land cover types, and support data in the form of aerial photographs and/or field observations. As a spatially and numerically continuous variable, NDVI can be readily combined with other spatially distributed variables such as PAR and  $T_s$  as input to empirical models for estimating regional CO<sub>2</sub> flux (Shippert et al., 1995). Vegetation/land cover type maps enable a partitioning of the land surface into cover type units, such that imbedded mechanistic or phenomenological models may operate for each unit and then be summed for an entire region (Oechel et al., 1996). As a hybrid of these two modeling approaches, NDVI maps derived from multitemporal satellite data, such as NOAA-AVHRR data acquired throughout a growing season, can be incorporated into imbedded models associated with cover type units, to provide information on seasonal dynamics of net primary productivity and possibly, ecosystem respiration (Markon et al., 1995).

Based on analysis of semi-variograms generated for SPOT-NDVI data (20 m spatial resolution), most of the vegetation cover and landform features of the arctic tundra landscape within our study area have spatial dimensions of less than 1 km. Thaw lakes on the coastal plain and glacial depositional landforms such as moraines in the foothills, seem to be the largest features (Dean and Morrissey, 1988). Vegetation units appear to have dimensions no larger than 700 m. The presence of a nugget effect in all of the variograms indicated that, even at the 20 m sample scale, higher frequency landscape features such as patterned ground and vegetation patches influence NDVI variability. The implications of the above on satellite-derived NDVI are that: (1) most fine-scale geomorphic features and associated vegetation patterns are integrated (averaged) within and vegetation units are much larger than the ground resolution element of moderate-resolution satellite sensors (e.g. SPOT and Landsat), and (2) almost all landscape features are smaller than the ground resolution element of NOAA-AVHRR.

The implication of (2) above is that NDVI from AVHRR will generally be influenced by mixtures of vegetation units and landform features. Whereas regression relationships established at the 1–10 m scale suggest that NDVI, standardized by PAR, is a good predictor of net ecosystem exchange of CO<sub>2</sub> (Whiting et al., 1992; McMichael, 1995), extending

this relationship to 1–3 km AVHRR-NDVI data may not be straightforward, because of these mixtures. Of particular importance is the influence of surface water proportions on AVHRR-NDVI and any empirical estimates of CO<sub>2</sub> based on AVHRR-NDVI data will likely require an adjustment for the proportion of water bodies within a pixel. Surface water covers large portions of the entire North Slope immediately following snowmelt and much of the coastal plain throughout the snow-free season. Some of our short-term research objectives are to explore the application of mixture models for estimating water proportions in AVHRR pixels and determine if a procedure of water-normalization is necessary for deriving stable NDVI values and associated estimates of CO<sub>2</sub> flux.

Our qualitative comparison of NDVI from spectral radiometers on fixed-wing aircraft (Stow et al., 1993b) and from AVHRR with measurements of CO<sub>2</sub> flux acquired by the NOAA-ATDD aircraft system along the two N–S transects shows strong similarities in spatial patterns and variability. Though this comparison is cursory and more rigorous, quantitative analyses will be conducted by the NSF LAII-FLUX study team, three distinctive NDVI-CO<sub>2</sub> flux zones associated with the two physiographic provinces and a transition zone are evident. The similarity in the trends provides further evidence that NDVI may be a good predictor of CO<sub>2</sub> flux. We will focus subsequent analyses on attempting to explain the large and infrequent deviations from the trend (likely associated with water bodies), as well as fluctuations in the CO<sub>2</sub> flux trend relative to the trend of NDVI. We have demonstrated in this paper that frequency distributions of satellite-derived NDVI provide information on whether aircraft-based CO<sub>2</sub> flux sampling schemes adequately capture the distribution of flux regimes within a regime. We have also demonstrated that regional pattern of NDVI for the North Slope of Alaska corresponds to differences between the two major physiographic provinces of this region.

#### **Acknowledgements**

This research was funded by the National Science Foundation's Office of Polar Programs as part of the

Arctic Systems Science, Land–Air–Ice Integration FLUX study (Walt Oechel, San Diego State University Principal Investigator). Computational facilities were provided by the San Diego Supercomputer, La Jolla, California. Dongmei Chen coded semi-variogram routines and John Helly provided supercomputer support. Tim Crawford and Steve Brooks of the National Oceanic and Atmospheric Administration (NOAA) Atmospheric Turbulence and Diffusion Division (ATDD) provided aircraft CO<sub>2</sub> flux data. Lloyd Coulter assisted with graphic production.

## References

- Belchansky, G.I., Ovchinnikov, G.K., Douglas, D.C., 1995. Comparative evaluation of ALMAZ, ERS-1, JERS-1, and Landsat-TM for discriminating wet tundra habitats. *Polar Record* 31, 161–168.
- Chavez, P.S. Jr., 1988. An improved dark-object subtraction technique for atmospheric scattering correction of multispectral data. *Remote Sensing Environm.* 24, 459–479.
- Cohen, W.B., Spies, T.A., Bradshaw, G.A., 1990. Semivariograms of digital imagery for analysis of conifer canopy structure. *Remote Sensing Environm.* 34, 167–178.
- Curran, P.J., 1988. The semi-variogram in remote sensing. *Remote Sensing Environm.* 24, 493–507.
- Davis, F.W., Dubayah, R., Dozier, J., Hall, F.G., 1989. Covariance of Greenness and Terrain Variables over the Konza Prairie. *Proceedings of International Geoscience and Remote Sensing Symposium*, Vancouver, BC.
- Dean, K.G., Morrissey, L.A., 1988. Detection and identification of arctic landforms: An assessment of remotely sensed data. *Photogramm. Eng. Remote Sensing* 54, 363–371.
- Fung, I.Y., Tucker, C.J., Prentis, K.C., 1987. Application of advanced very high resolution radiometer vegetation index to study atmosphere–biosphere exchange of CO<sub>2</sub>. *J. Geophys. Res.* 92, 2999–3015.
- Hamilton, T.D., 1986. Late Cenozoic glaciation of the Central Brooks Range. In: Hamilton, T.D., Thorson, R.M. (Eds.), *Glaciation in Alaska: The Geologic Record*. Alaska Geological Society, Anchorage, pp. 9–49.
- Hope, A.S., Fleming, J.B., Vourlitis, G., Stow, D.A., Oechel, W.C., Hack, T., 1995. Relating CO<sub>2</sub> fluxes to spectral vegetation indices in tundra landscapes: Importance of footprint definition. *Polar Record* 31, 245–250.
- Hope, A.S., Kimball, J.S., Stow, D.A., 1993. The relationship between tussock tundra spectral reflectance properties and biomass and vegetation composition. *Int. J. Remote Sensing* 14, 1861–1874.
- Markon, C., Fleming, M.D., Binnian, E.F., 1995. Characteristics of vegetation phenology over the Alaskan landscape using AVHRR time-series data. *Polar Record* 31, 179–190.
- McMichael, C.E., 1995. Estimating CO<sub>2</sub> Exchange in Arctic Tundra Ecosystems Using a Spectral Vegetation Index. Unpublished MA thesis, Department of Geography, San Diego State University, San Diego, California.
- Morrissey, L.A., Livingston, G.P., 1992. Methane emissions from Alaska arctic tundra: An assessment of local spatial variability. *J. Geophys. Res.* 97-D15, 16661–16670.
- Oechel, W.C., Vourlitis, G.L., 1996. Direct effects of elevated CO<sub>2</sub> on arctic plant and ecosystem function. In: Koch, W., Mooney, H. (Eds.), *Terrestrial Ecosystem Response to Elevated Carbon Dioxide*, Academic Press, San Diego, pp. 163–174.
- Oechel, W.C., Hastings, S.J., Vourlitis, G., Jenkins, M., Riechers, G., Grulke, N., 1993. Recent change of arctic tundra ecosystems from a net carbon dioxide sink to a source. *Nature* 361, 520–523.
- Oechel, W.V., Vourlitis, G.L., Gilmanov, T., Nosov, V., Stow, D., Hope, A., Brooks, S., Crawford, T., Dumas, E., McGillen, T., Kane, D., Hinzman, L., 1996. CO<sub>2</sub> Flux from Arctic Tundra Measured at Three Scales by Chamber, Eddy Correlation Tower, and Aircraft Techniques and Extrapolation to a Watershed Scale. In: Panikov, N.S. (Ed.), *Annals of Geophysics XXII, European Geophysical Union General Assembly, May 5–10, 1995, The Hague, The Netherlands*. Chapman & Hall, London, 378 pp.
- Shasby, M., Carneggie, D., 1986. Vegetation and terrain mapping in Alaska using Landsat MSS and digital terrain data. *Photogramm. Eng. Remote Sensing* 52, 779–786.
- Shippert, M.M., Walker, D.A., Auerbach, N.A., Lewis, B.E., 1995. Biomass and leaf-area index maps derived from SPOT images for Toolik Lake and Imnavait Creek areas, Alaska. *Polar Record* 31, 147–154.
- Stow, D., Burns, B., Hope, A., 1989. Mapping Arctic tundra vegetation types using digital SPOT/HRV-XS data: a preliminary assessment. *Int. J. Remote Sensing* 10 (8), 1451–1457.
- Stow, D.A., Burns, B.H., Hope, A.S., 1993a. Spectral, spatial and temporal characteristics of arctic tundra reflectance. *Int. J. Remote Sensing* 14, 2445–2462.
- Stow, D.A., Hope, A.S., George, T.H., 1993b. Reflectance characteristics of arctic tundra vegetation from airborne radiometry. *Int. J. Remote Sens.* 14, 1239–1244.
- Tucker, C.J., Fung, I.Y., Keeling, C.D., Gammon, R.H., 1986. Relationship between atmospheric CO<sub>2</sub> variations and a satellite-derived vegetation index. *Nature* 319, 195–199.
- Tucker, C.J., Sellers, P.J., 1986. Satellite remote sensing of primary production. *Int. J. Remote Sensing* 7, 1395–1416.
- Vierling, L.A., Deering, D.W., Eck, T.F., 1997. Nadir and bi-directional surface radiometric measurements of arctic tundra: Site differentiation and vegetation phenology early in the growing season. *Remote Sensing Environm.* 60, 71–82.
- Vourlitis, G., Oechel, W.C., 1997. The role of northern ecosystems in the global methane budget. In: Oechel, W.C., Callaghan, T., Elling, H., Gilmanov, T., Holten, J.I., Maxwell, B., Molau, U., Rogne, O., Sveinbjornsson, B. (Eds.), *Global Change and Arctic Terrestrial Ecosystems: An International Conference*, Springer, Berlin, pp. 266–289.
- Walker, D.A., Walker, M.D., 1991. History and pattern of distur-

- bance in Alaskan arctic ecosystems: a hierarchical approach to analyzing landscape change. *J. Appl. Ecol.* 28, 244–276.
- Walker, D.A., Walker, M.D., 1996. Terrain and vegetation of the Imnavait Creek watershed. In: Reynolds, J.F., Tenhunen, J.D. (Eds.), *Landscape Function and Disturbance in Arctic Tundra*. Ecological Studies, Springer, Berlin, pp. 73–108.
- Walker, D.A., Acevedo, W., 1987. Vegetation and a Landsat-derived land cover map of the Beechey Point Quadrangle, Arctic Coastal Plain, Alaska. U.S. Army Cold Regions Engineering and Research Laboratory, Hanover, NH, CRREL Report 87-5, 63 pp.
- Walker, D.A., Auerbach, N.A., Shippert, M.M., 1995a. NDVI, biomass, and landscape evolution of glaciated terrain in northern Alaska. *Polar Record* 31, 169–178.
- Walker, D.A., Bay, C., Daniels, F.J.A., Einarsson, E., Elvebakk, A., Johansen, B.E., Kapitsa, A., Kholod, S.S., Murray, D.F., Talbot, S.S., Yurtsev, B.A., Zoltai, S.C., 1995b. Toward a new arctic vegetation map: A review of existing maps. *J. Vegetat. Sci.* 6, 427–436.
- Weller, G., Chapin, F.S., Everett, K.R., Hobbie, J.E., Kane, D., Oechel, W.C., Ping, C.L., Reeburgh, W.S., Walker, D., Walsh, J., 1995. The Arctic Flux study: a regional view of trace gas release. *J. Biogeogr.* 22, 365–374.
- Whiting, G.J., Bartlett, D.S., Fan, S., Bawkin, P.S., Wofsy, S.C., 1992. Biosphere/atmosphere CO<sub>2</sub> exchange in tundra ecosystems: community characteristics and relationships with multi-spectral surface reflectance. *J. Geophys. Res.* 97, 16671–16680.
- Woodcock, C.E., Strahler, A.H., Jupp, D.L.B., 1988. The use of variograms in remote sensing 1. Scene models and simulated images. *Remote Sensing Environm.* 25, 323–348.